NONADIABATIC QUANTUM WAVE-PACKET DYNAMICS OF ATOM-DIATOM REACTIONS

A Thesis

Submitted for the Degree of

DOCTOR OF PHILOSOPHY

By

B. JAYACHANDER RAO

SCHOOL OF CHEMISTRY

UNIVERSITY OF HYDERABAD

HYDERABAD - 500 046

INDIA

December 2007

Contents

Appendix A

On the $(E \otimes e)$-Jahn-Teller conical intersections in the 3p (E') and 3d (E'') Rydberg electronic states of triatomic hydrogen

A.1 Introduction

We present and discuss the static and dynamic aspects of the Jahn-Teller (JT) interactions in the 3p (E') and 3d (E'') Rydberg electronic states of H_3 in this chapter theoretically. The static aspects are discussed based on recent ab initio quantum chemistry results, and the dynamic aspects are examined in terms of the vibronic spectra and nonradiative decay behavior of these states. The adiabatic potential energy surfaces of these degenerate electronic states are derived from extensive *ab initio* calculations. The calculated adiabatic potential energy surfaces are diabatized following our earlier study [168] on this system in its 2p (E')

ground electronic state. The nuclear dynamics on the resulting conically intersecting manifold of electronic states is studied by a time-dependent wave packet approach. Calculations are performed both for the uncoupled and coupled state situations in order to understand the importance of nonadiabatic interactions due to the JT conical intersections in these excited Rydberg electronic states.

The ab initio adiabatic potential energies of the JT split components of the 3p (E') , 3d (E'') and several other excited Rydberg electronic states of H_3 were calculated over a large number of geometrical arrangements by Jungen and coworkers [169]. The resulting adiabatic PESs are diabatized and the nuclear motion on the coupled diabatic surfaces is monitored by a time-dependent WP approach. The vicinity of the D_{3h} equilibrium geometry of Rydberg excited H_3 is probed by the electron collision of H_3^+ in molecular beams [93, 94]. Therefore, it is valuable to understand the topography of the PESs of the 3p (E') and 3d (E'') electronic states in the neighborhood of the D_{3h} configuration and the motion of the WP on them (these two states have major contributions to the Rydberg emission process [93, 94]). Like the 2p (E') ground electronic manifold, these two degenerate Rydberg excited states are also prone to the JT instability [6]. Investigations of the impact of the JT coupling on the spectroscopy and nonradiative decay of these states are the two main aspects of the present investigation.

The conical intersections of the JT split 3p (E') and 3d (E'') Rydberg electronic states are established. Our analysis shows that the JT interactions are not particularly strong in these electronic states, when compared to that in the electronic ground state of H_3 [95, 168, 170]. In the following, we consider both the uncoupled and coupled state situations and examine the vibronic level structure of these electronic states. The nonradiative decay of these states is examined by calculating the time-dependent adiabatic and diabatic electronic populations.

The results show much slower decay rates of these Rydberg states when compared with the same of the electronic ground state [95, 168].

A.2 Diabatic electronic states and conical intersections

The adiabatic potential energy surfaces used in this paper are a subset of solutions from a large number of geometrical arrangements where the lowest 15 electronic states have been documented between the geometry of H_3^+ and the dissociation limit to H + H_2 [169]. An orbital basis of 165 contracted Gaussian functions has been used which can describe Rydberg dissociation to H^* + H_2 as well as to H + H_2^*. At every grid point a CI (Configuration Interaction) calculation in the dimension of about 14000 CSF's (Configuration State Function) has been performed and calculations for 2366 grid points have been carried out.

The internal coordinates of H_3 have been chosen as mass scaled Jacobi coordinates R, r and γ with

$$R = S \cdot 0.75^{-1/4} \tag{A.1a}$$

$$r = s \cdot 0.75^{1/4}. \tag{A.1b}$$

Here s is the H-H distance in the diatom, S is the distance between the third H atom and the center of mass of the diatom, and γ is the angle between the vectors $\vec{r}$ and $\vec{R}$. For the equilibrium geometry of H_3^+ (an equilateral triangle with interatomic distances of 1.65 a_0) we have $R = r = 1.536\ a_0$ and $\gamma = 90°$. Our

grid has been chosen such that one point exactly coincides with this equilibrium ; the step size is 0.2 a_0 for R and r in the vicinity of the H_3^+ minimum, 0.4 a_0 at longer separations, and 15° for γ. In the following these internal coordinates will also be used for the treatment of the nuclear dynamics.

In contrast to the 2p (E') surfaces the potentials of the 3p (E') state have an absolute minimum near the geometry of H_3^+. It is a double surface which in D_{3h} symmetry penetrates itself. Close to the minimum the surfaces are roughly parallel to that of the parent ion, but in C_{2v} symmetry ($\gamma = 90°$) the higher component of the 3p (E') surfaces has a saddlepoint near $R \sim 1.0$ a_0, $r \sim 2.6$ a_0, about 1.3 eV above the minimum; near $R \sim 0.9$ a_0, $r \sim 2.9$ a_0 it intersects the lower component such that in a linear arrangement (R =0) their sequence is inverted for $r > 3.0$ a_0.

The surfaces of the 3d (E'') state are embedded in a dense sequence of electronic states, together with 3s (A_1'), 3p (A_2''), 3d (E') and 3d (A_1'). At the equilibrium these 7 states are compressed into an energy interval of about 0.1 eV, much less than the typical zero point vibrational energies in these potentials (0.54 eV for H_3^+). The potential surfaces are qualitatively parallel to that of the parent ion and the 3d (E'') surfaces are not intersected by another potential up to an energy of about 1 eV above the minimum.

We utilized the above adiabatic potential energy data for the 3p (E') and 3d (E'') electronic states and diabatized them using a very simple approach [21–23]. In this approach the leading derivative coupling elements of the adiabatic basis, i.e., those which diverge at a conical intersection are removed [22]. It is shown that for a symmetry-enforced ($E \times e$)-JT conical intersection, much simplification results in the construction of the diabatic electronic states [22]. In this case the adiabatic-to-diabatic mixing angle is solely determined in a geometrical fashion

and does not depend at all on the strength of the JT coupling. This is already been exploited in our earlier works on this system [24,95,168,170] and encouraging results thereof emerged. If the two adiabatic components of the JT split potential energy surfaces are designated V_- (lower) and V_+ (upper) then the diabatization scheme reads

$$\begin{pmatrix} U_{11} & U_{12} \\ U_{21} & U_{22} \end{pmatrix} = \mathcal{S} \begin{pmatrix} V_- & 0 \\ 0 & V_+ \end{pmatrix} \mathcal{S}^\dagger \tag{A.2}$$

$$= \frac{V_- + V_+}{2}\mathbf{1} + \frac{V_+ - V_-}{2} \begin{pmatrix} -\cos\chi & \sin\chi \\ \sin\chi & \cos\chi \end{pmatrix}, \tag{A.3}$$

with

$$\mathcal{S} = \begin{pmatrix} \cos\phi & \sin\phi \\ -\sin\phi & \cos\phi \end{pmatrix}. \tag{A.4}$$

U_{11} and U_{22} represent the two diabatic potential energy surfaces and, $U_{12} = U_{21}$, is their coupling surface. The quantity $\mathcal{S}$ defines the unitary transformation matrix from the adiabatic to the diabatic representation; $\Psi^{diab} = S\ \Psi^{adiab}$; ϕ is the adiabatic-to-diabatic mixing angle given by [10]

$$\sin(2\phi) = \frac{U_{12}}{\sqrt{\Delta^2 + U_{12}^2}}, \tag{A.5}$$

$$\cos(2\phi) = \frac{\Delta}{\sqrt{\Delta^2 + U_{12}^2}}, \tag{A.6}$$

with

$$\Delta = \frac{U_{22} - U_{11}}{2} \tag{A.7}$$

When expressed in terms of the adiabatic surfaces V_- and V_+, the elements of the electronic Hamiltonian matrix read,

$$U_{11} = \overline{V} - \delta \cos\chi \tag{A.8}$$

$$U_{22} = \overline{V} + \delta \sin\chi \tag{A.9}$$

$$U_{12} = U_{21} = \delta \sin\chi \tag{A.10}$$

where $\overline{V} = (V_- + V_+)/2$ and $\delta = (V_+ - V_-)/2$ and $\chi = 2\phi$.

The quantity χ above is the pseudorotation angle defined to be the polar angle of the e-type vibration in the two-dimensional vibrational subspace of the system. It can be seen that the above diabatization scheme requires information on the adiabatic potential energies V_- and V_+ of the system only. This is a very simple scheme, but, has been shown to remove the leading derivative coupling terms that exhibit singular behavior at the conical intersections [21–23].

The computed adiabatic points on a (R, r, γ) grid by Jungen and coworkers are used here [169]. The raw adiabatic data are used to calculate the diabatic potential energies at each point of the grid and the resulting diabatic surfaces are then numerically interpolated using a three-dimensional spline on a denser grid. The numerical WP calculations are carried out on the latter consisting of a uniformly spaced 128 × 128 grid in the (R, r) plane with $0.33a_0 \leq R \leq 5.13a_0$ and $1.13a_0 \leq r \leq 5.13a_0$ (for the 3p (E') electronic manifold) and $0.33a_0 \leq R \leq 3.13\ a_0$, $1.13a_0 \leq r \leq 2.33a_0$ (for the 3d (E'') electronic manifold). A 63 point Gauss-Legendre quadrature [152] is used for γ in both cases. Unlike the adiabatic potential energy functions, the diabatic potential energy functions do not exhibit a cusp like behavior at the seam of conical intersections [10]. Therefore, it is much simpler to numerically interpolate the diabatic potential energy functions

rather than the adiabatic ones.

The two diabatic components of the 3p (E') Rydberg electronic manifold of H_3 are shown in Figs. 1(a-b) and indicated by the thin and thick lines. The contour lines in panel a are plotted in the (R, r) plane for $\gamma = \pi/2$ corresponding to the C_{2v} arrangements of the three nuclei. The seam of the $(E \times e)$-JT conical intersections occurring for $R = r$ is shown by the line on the diagram. H_3 possesses an equilateral triangular geometry on this line. The energetic minimum on the seam is indicated by the cross. This minimum occurs at $R = 1.56\ a_0$, $r = 1.56\ a_0$ and $\gamma = \pi/2$. This minimum point on the seam is more clearly shown in panel b and indicated by an arrow. The energy at this minimum of the seam is ~ 2.43 eV relative to the three-body dissociation (H+H+H) limit [1] .

The above two diabatic potential energy surfaces obtained from the computed adiabatic potential energy data (panels in the left column) and the corresponding interpolated ones (panels in the right column) on the denser grid (defined above) using a three-dimensional spline are shown in the (R, r) plane in Figs. 2(a-c) for $\gamma = 0°$, $30°$ and $60°$, respectively. The two diabatic electronic states are indicated by two different line types in the figure.

It can be seen from the figures that the interpolated diabatic surfaces represent quite well the raw data, and are very smooth. The coupling surfaces of the above two diabatic surfaces are shown as contour line diagrams in the (R, r) plane in Figs. 3 (a-c) for $\gamma = 0°$, $30°$ and $60°$, respectively. The raw data and the corresponding interpolated ones are shown in the left and right column of the figure, respectively. A smooth behavior of the coupling surfaces is also apparent from the figure. It is to be noted that the coupling energy is exactly zero for the C_{2v} arrangements of the nuclei. The magnitude of the coupling potential becomes

[1] Improved energies will be introduced at the end of section IV B

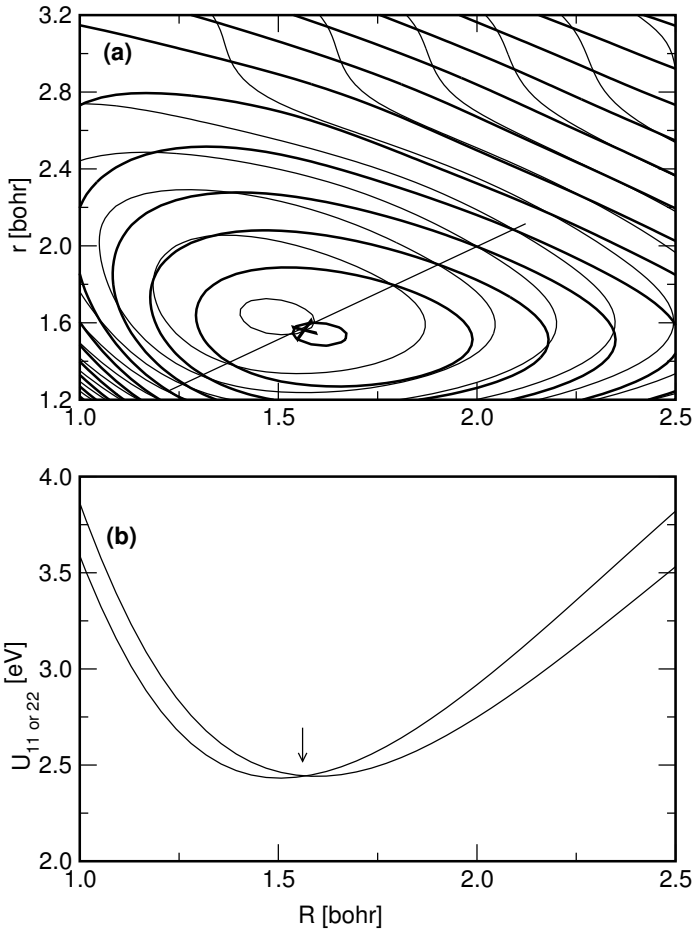

Figure A.1: (a) Contours of the potential energies (eV) of the two diabatic components of the 3p (E') Rydberg electronic manifold of H_3 plotted in the (R, r) plane for $\gamma{=}\pi/2$. The lowest energy contour for both the states occurs at 2.45 eV and the spacing between the successive lines is 0.3 eV. The energy is measured relative to the three-body dissociation (H + H + H) limit. The straight line in the figure indicates the seam of conical intersections (occurring for $R = r$ between these two component states). The location of the energetic minimum on this seam is shown by the cross. (b) Potential energy cuts of the above two diabatic electronic states along R through the minimum of the seam of conical intersections. The minimum of the seam is indicated by an arrow and the minimum energy amounts to 2.43 eV.

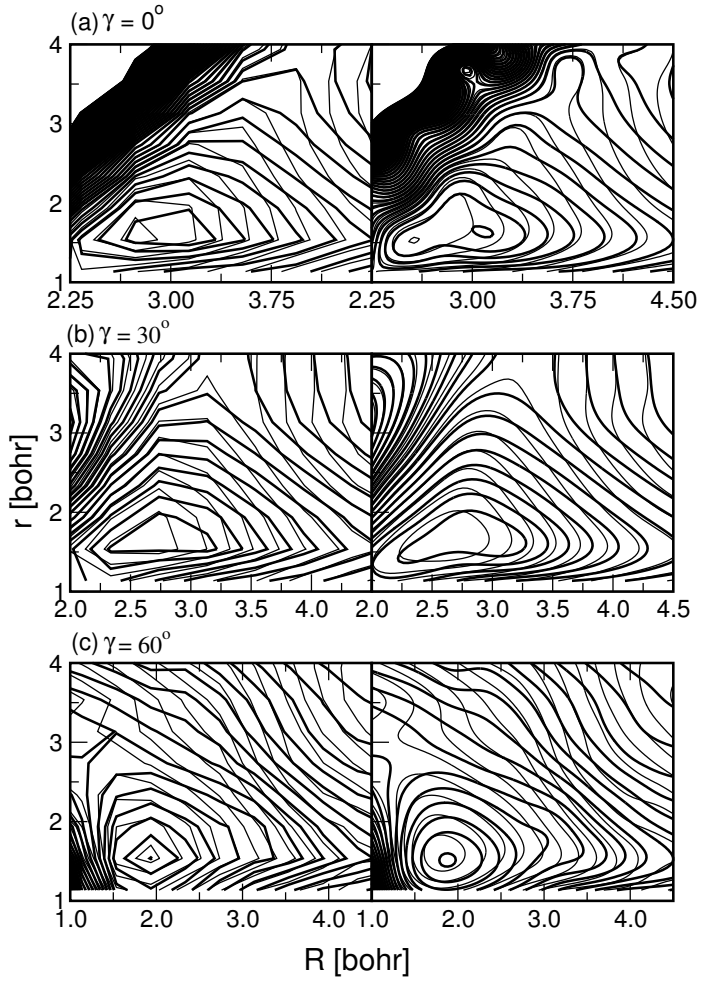

Figure A.2:

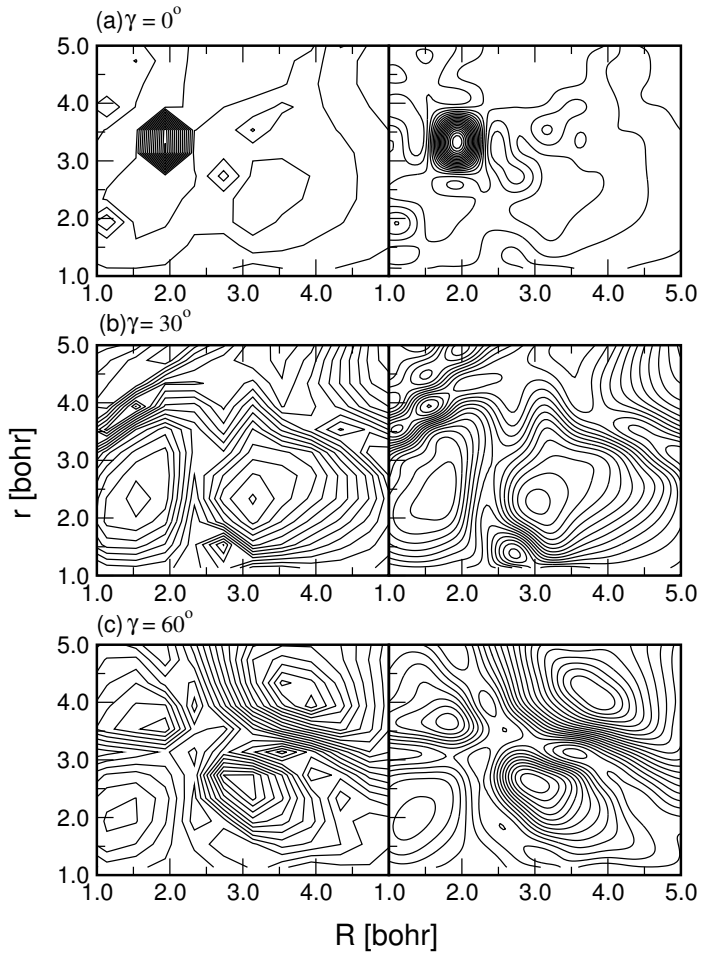

Figure A.3:

maximum at $\gamma = 0$ or π. Typically for the 3p (E') electronic state the maximum value is ~ 0.78 eV, occurring for $R \sim 3.43\ a_0$, $r \sim 5.04\ a_0$ and $\gamma \sim 0$ or π.

The two component diabatic potential energy surfaces of the 3d (E'') Rydberg electronic manifold of H_3 are plotted in the (R, r) plane for $\gamma = \pi\ /2$ and are shown in Fig 4(a). It can be seen that the topography of these two diabatic states is very similar and they remain energetically very close even for geometries far away from the D_{3h} configurations. This indicates that the JT interaction in the 3d (E'') electronic manifold is weaker than that in the 3p (E') electronic manifold.

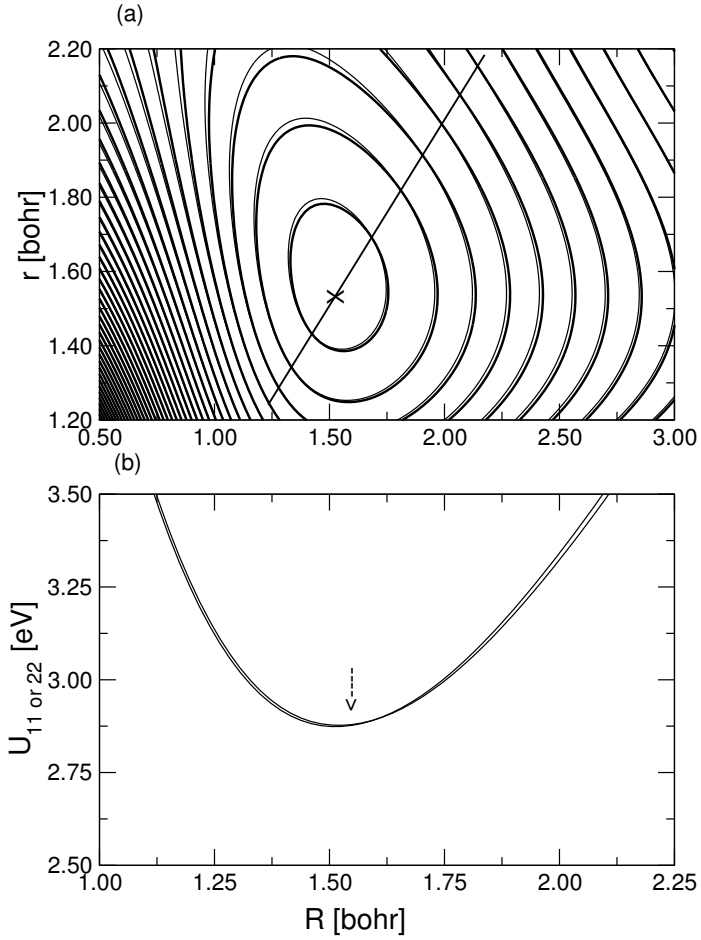
(a)
2.20
2.00
1.80
1.60
1.40
1.20
r [bohr]
0.50
1.00
1.50
2.00
2.50
3.00
(b)
3.50
3.25
3.00
2.75
2.50
U11 or 22 [eV]
1.00
1.25
1.50
1.75
2.00
2.25
R [bohr]

Figure A.4:

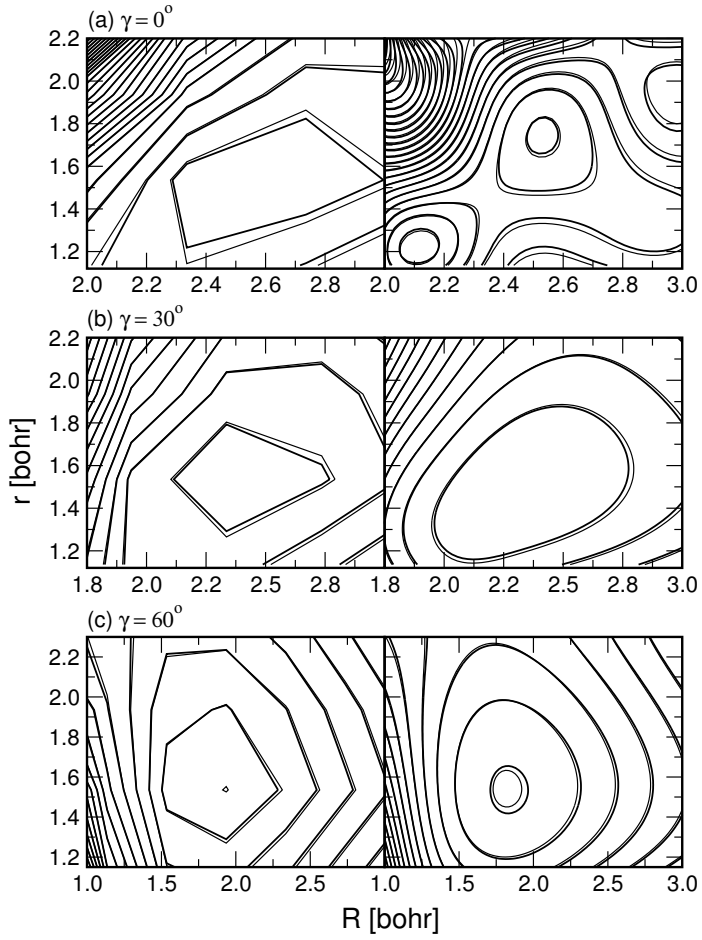

Figure A.5:

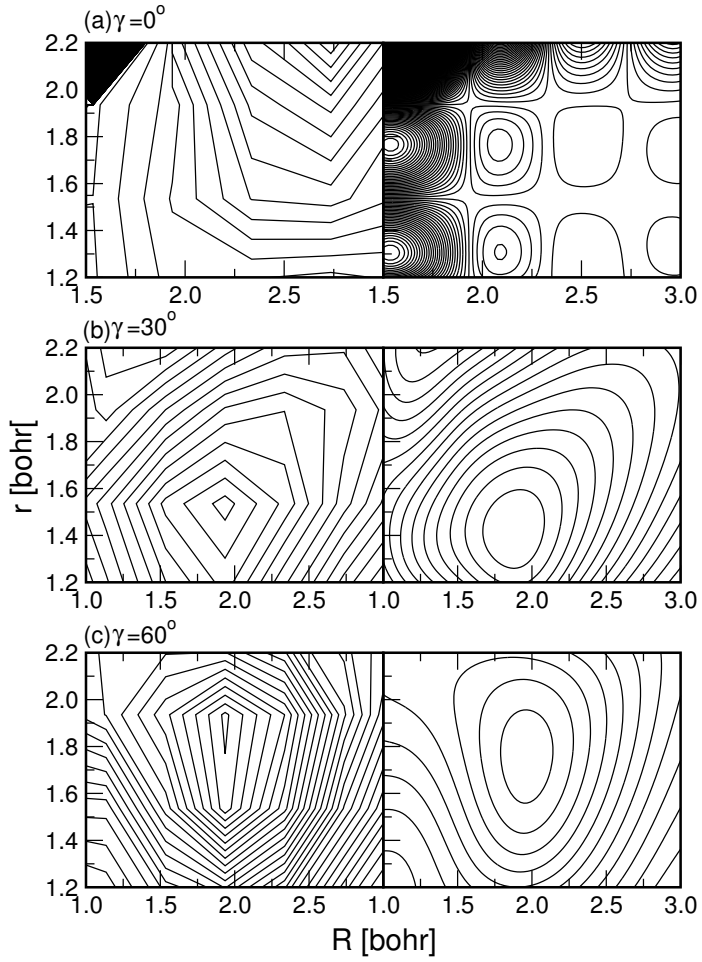

Figure A.6:

The seam of conical intersections in the 3d (E'') electronic manifold is indicated by the straight line in Fig. 4(a). The energetic minimum on this seam is marked by the cross on the diagram. This minimum occurs at $R = 1.52\ a_0$, r= 1.52 a_0 and $\gamma = \pi/2$. The cuts of the above two diabatic surfaces through this minimum along R is shown in panel b. The minimum is more clearly shown by an arrow in the diagram and the energy at this minimum is $\sim$ 2.87 eV relative to the H + H + H dissociation limit. The maximum magnitude of the coupling potential in this case is 0.31 eV. We note that the coupling potential has a maximum value $\sim$ 3.25 eV for the 2p (E') ground electonic manifold of H_3. Therefore, it appears that the JT effects are much weaker in the Rydberg electronic states compared to those in the ground electronic manifold.

In order to show the quality of the numerical interpolations, we show in Figs. 5(a-c) the cuts of the component diabatic states of the 3d (E'') electronic manifold in the (R, r) plane and for $\gamma = 0°$, $30°$ and $60°$, respectively. The coupling potentials of these two states are shown in Figs. 6(a-c) for $\gamma = 0°$, $30°$ and $60°$, respectively. The diabatic energies and the coupling potentials derived from the computed ab initio adiabatic potential energies are shown in the left and the corresponding interpolated surfaces are shown in the right columns of Fig. 5 and Fig. 6. A smooth behavior of the diabatic surfaces and their coupling surfaces is also apparent in this case.

A.3 Theoretical framework to treat the nuclear dynamics

The nuclear dynamics in the degenerate 3p (E') and 3d (E'') Rydberg electronic states H_3 is expected to be influenced by the low-lying conical intersections in

these states. For propagation of wave packets in these electronic states, we resort to the diabatic electronic basis discussed above. In this basis the coupling surfaces exhibit a smooth behavior rather than a singularity as in the adiabatic electronic basis [10]. The vibronic Hamiltonian in the diabatic electronic basis can be written as

$$\mathcal{H} = \mathcal{T}_{\mathcal{N}} \begin{pmatrix} 1 & 0 \\ 0 & 1 \end{pmatrix} + \begin{pmatrix} U_{11} & U_{12} \\ U_{21} & U_{22} \end{pmatrix}, \tag{A.11}$$

where T_N represents the nuclear kinetic energy operator, which is diagonal in this basis. In terms of the mass-scaled body-fixed (BF) Jacobi coordinates R, r and γ (introduced in Sec. II) and for the total angular momentum $\mathbf{J} = 0$, it is given by [181]

$$\mathcal{T}_{\mathcal{N}} = -\frac{\hbar^2}{2\mu}\left[\frac{\partial^2}{\partial R^2} + \frac{\partial^2}{\partial r^2}\right] - \frac{\hbar^2}{2I}\frac{1}{\sin\gamma}\frac{\partial}{\partial\gamma}\left(\sin\gamma\frac{\partial}{\partial\gamma}\right). \tag{A.12}$$

The quantity, $\mu = m_H/\sqrt{3}$, above is the three-body scaled reduced mass and, $I = (\mu R^2 r^2)/(R^2 + r^2)$, is the moment of inertia. The BF z-axis is defined to be parallel to $\vec{R}$ and the diatom lies in the (x, z) plane.

In the time-dependent picture the golden rule expression for the spectral intensity is given by

$$P(E) \approx Re\int_0^\infty e^{iEt/\hbar}\langle\psi(0)|e^{-i\mathcal{H}t/\hbar}|\psi(0)\rangle dt, \tag{A.13}$$

where $\psi(0)$ defines the initial wave function of the system. In the present application, this function can be assumed to be prepared by the Franck-Condon transition of a hypothetical initial state to the coupled manifold of final degenerate electronic states. This is in the spirit of transition state spectroscopy, but

utilizing hypothetical initial wave packets as specified below. In this sense Eq. (14) above represents a pseudospectral intensity. In a vector notation the initial wave function can be given as

$$\psi(0) \;=\; \psi_1(R,r,\gamma)\begin{pmatrix}1\\0\end{pmatrix} + \psi_2(R,r,\gamma)\begin{pmatrix}0\\1\end{pmatrix}, \tag{A.14}$$

where $\begin{pmatrix}1\\0\end{pmatrix}$ and $\begin{pmatrix}0\\1\end{pmatrix}$ indicates the first and the second diabatic electronic state with energy U_{11} and U_{22}, respectively. ψ_1 and ψ_2 are the nuclear wave functions in the respective diabatic states depending on the set of Jacobi coordinates. In the present study we have chosen a Gaussian wave packet (GWP) for ψ_1 and ψ_2,

$$\begin{aligned}\psi_{1,2} \;=\; & N\exp\left[-\frac{(R-R^0)^2}{2\sigma_R^2} - \frac{(r-r^0)^2}{2\sigma_r^2}\right] \\ & \times\left\{\exp\left[\frac{(\gamma-\gamma^0)^2}{2\sigma_\gamma^2}\right] + \exp\left[\frac{(\gamma-\pi+\gamma^0)^2}{2\sigma_\gamma^2}\right]\right\}.\end{aligned} \tag{A.15}$$

The quantities R^0, r^0 and γ^0 specify the initial location and σ_R, σ_r and σ_γ refer to the width parameters of the GWP along the respective coordinates. All the vibronic energy levels of the system can be obtained with appreciable intensities by suitably varying the initial location and the width parameters of this GWP. The initial parameters and the average energies of the GWPs used in the present calculations are given in Table I (for the 3p (E') electronic manifold) and Table II (for the 3d (E'') electronic manifold).

The action of the time evolution operator $e^{-i\mathcal{H}t/\hbar}$ on the initial wave function in Eq. (14) is evaluated by dividing the time axis into n segments of length Δt. The exponential operator at each time step Δt is then approximated by the split-operator method [137]. For the spatial evolution of the WP we used the

fast Fourier transform method [144] for the radial kinetic energy operators and a discrete variable representation [145] for the angular kinetic energy operator. In each calculation the WP is evolved for a total time of 2.2 ps with a step length of Δt = 0.135 fs (3p (E') electronic manifold) and 550 fs with a step length of Δt = 0.135 fs (3d (E'') electronic manifold). The fast moving components of the WP reaching the grid edges are absorbed by activating a sin-type masking function [149] at $R_{mask} = 4.15\ a_0$, $r_{mask} = 4.13\ a_0$ in case of the 3p (E') electronic manifold and at $R_{mask} = 2.72\ a_0$, $r_{mask} = 2.23\ a_0$ in case of the 3d (E'') electronic manifold, respectively. The convergence of the calculations is explicitly checked by varying the numerical grid parameters stated above.

A.4 Results and discussion

The focus of the present work is to investigate the nonadiabatic coupling effects on the WP dynamics of H_3 near the conical intersection of its 3p (E') and 3d (E'') Rydberg electronic states. This is motivated by our further plan to examine the dissociative recombination process of Rydberg excited H_3. In the coupled state calculations the WP is initially prepared on the adiabatic electronic state and then transformed to the diabatic electronic basis for the propagation and final analysis. Companion calculations are carried out for the uncoupled adiabatic electronic states in order to clearly reveal the impact of the ($E \times e$)-JT conical intersections on the vibronic structure of these degenerate Rydberg electronic states. Different initial locations of the GWP on the potential energy surface yield same eigenvalue spectra. However, the intensity of the peaks differs in different spectra. Therefore, by varying the initial location of the GWP (cf. Tables I & II) we are able to map out all the low-lying energy levels of the 3p (E') and 3d

(E'') electronic states with appreciable intensities. In the following, we show and discuss the results obtained with only one location of the GWP in each case.

A.4.1 Vibronic levels of the 3p (E') Rydberg electronic manifold

The pseudospectrum of the uncoupled lower (V_-) adiabatic sheet of the 3p (E') electronic manifold of H_3 obtained with the initial GWP No. 3 (cf. Table I) is shown in Fig. 7(a).

The peaks in the spectrum correspond to the bound vibrational energy levels of V_-. The energy is measured relative to the three-body dissociation (H + H + H) limit of 1.5 E_h. The energy eigenvalues and the assignments of the low-lying vibrational levels of V_- are given in Table III and are discussed below. The commonality of energy eigenvalues in various spectra obtained with different initial location of the GWP is explicitly checked. The pseudospectrum of V_- obtained with the GWP No. 3 in the coupled state situation is shown in Fig. 7(b). The discrete level structure of the uncoupled V_- (cf. Fig. 7(a)) becomes somewhat diffuse in the coupled state situations. The peak origin in the latter spectrum (cf. Fig. 7(b)) shifts by ~ 0.04 eV to higher energy which is due to the geometric phase effects arising from the sign change of the adiabatic electronic wave function while encircling the conical intersection in a closed loop [168,175]. The minimum of the seam of conical intersections in the 3p (E') electronic manifold occurs at ~ 2.43 eV. It can be seen that the 0-0 line in both the spectra in Fig. 7 appears above this energy. The energy eigenvalues of some of the distinct peaks in Fig. 7(b) are also given in Table III. It can be seen that the line density in the coupled state spectrum increases when compared to the uncoupled one. This increase is due to the nonadiabatic effects associated with the JT conical intersections in the

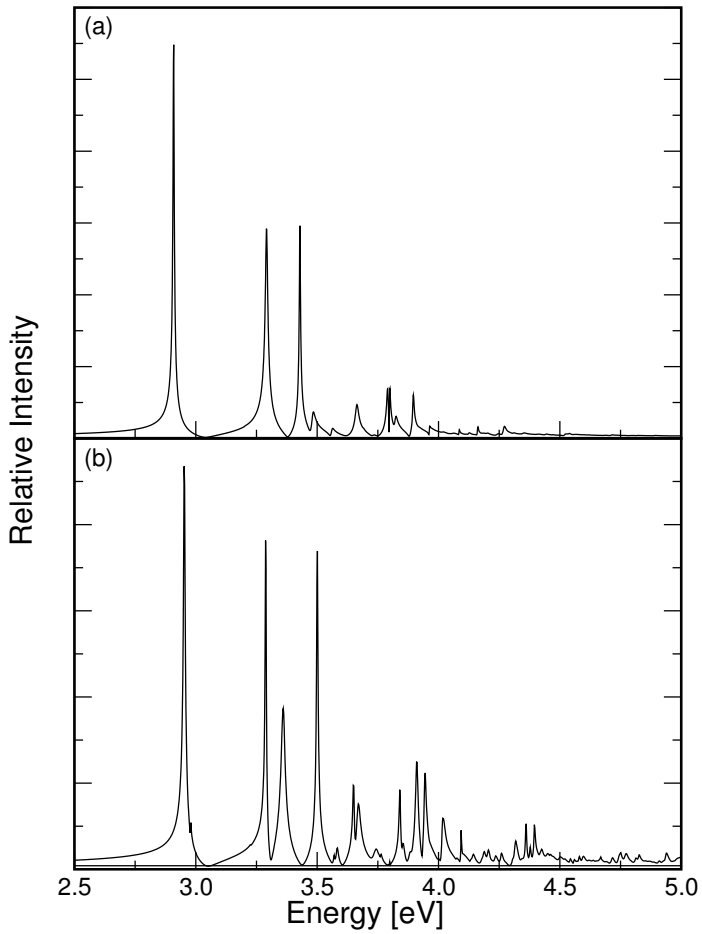

Figure A.7:

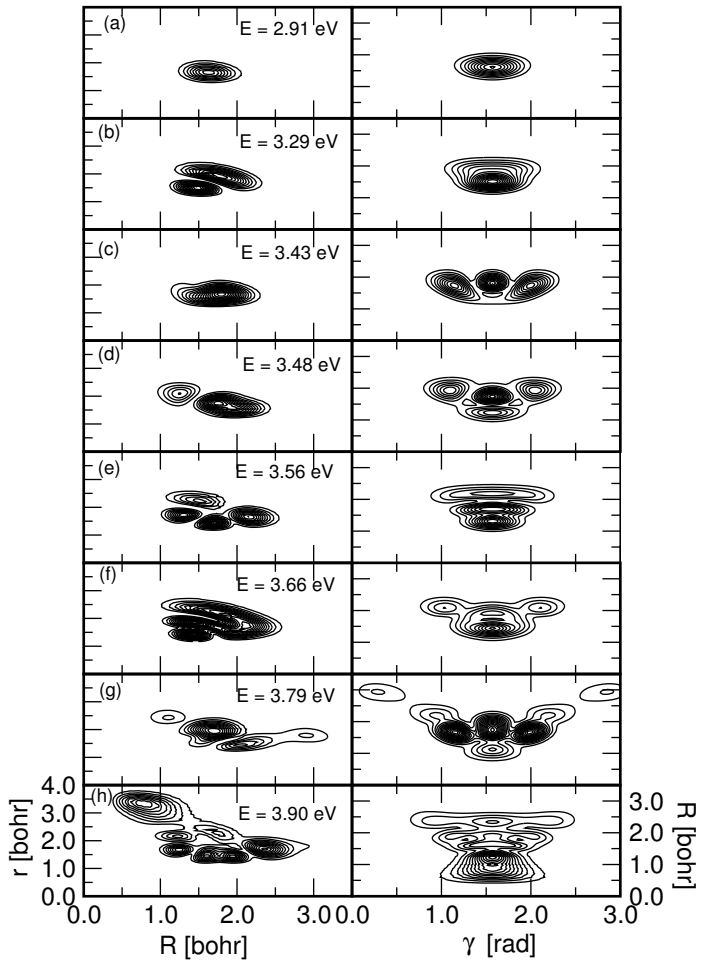

Figure A.8:

3p (E') electronic manifold [10]. The vibrational levels of the uncoupled V$_-$ in Fig. 7(a) are assigned by computing their eigenfunctions, by projecting the time evolved WP onto the desired eigenstate (n) of energy E_n,

$$\psi_n(E) = \int_0^\infty e^{iE_n t/\hbar}\psi(t)dt. \tag{A.16}$$

The vibrational eigenfunctions of the uncoupled V_- surface are shown in Figs. 8(a-h). Probability density ($|\psi_n(E)|^2$) contours of the eigenfunctions are plotted

in the (R, r) plane (panels in the left column) and (γ, R) plane (panels in the right column). The probability density is averaged over γ in the former case and over r in the latter case. The eigenfunctions are assigned in terms of the number of nodes, n_R, n_r and n_γ along R, r and γ, respectively. According to this prescription the eigenfunction in Fig. 8(a) would correspond to a (0,0,0) level. This is the ground vibrational level of the uncoupled V_- surface. The eigenfunction in Fig. 8(b) represents the (0,1,0) level and that in Fig. 8(c) the (0,0,2) level. The assignments of all the eigenfunctions in Figs. 8(a-h) are given in Table III. Even quantum excitation along the angle γ is seen in the eigenfunctions. In our previous work on the 2p (E') ground electronic state of H_3, we identified the eigenfunctions in terms of the progression along the breathing and bending vibrational modes [10]. These actually represent suitable linear combinations of the motions in Jacobi coordinates. Excitation along the breathing mode corresponds to a nodal progression along the D_{3h} symmetric stretch line ($R = r$). A nodal progression orthogonal to this line corresponds to the excitation along the bending mode. It is difficult to unambiguously assign the eigenfunctions in Fig. 8 according to this prescription due to their complex nodal pattern, however, the following qualitative estimates can be made. The eigenfunction in Fig. 8(b) corresponds to one quantum excitation along the degenerate bending vibrational mode. Therefore, one vibrational quantum of this mode is ~ 0.38 eV in the lower adiabatic sheet of the 3p (E') electronic manifold. Similarly, the eigenfunction in Fig. 8(f) has two quanta along this mode in addition to two quanta along γ. The eigenfunction in Fig. 8(e) corresponds to one quantum excitation along the breathing and one quantum along the degenerate bending vibrational mode. Therefore, the vibrational quantum along the breathing vibrational mode is $\sim$ 0.27 eV.

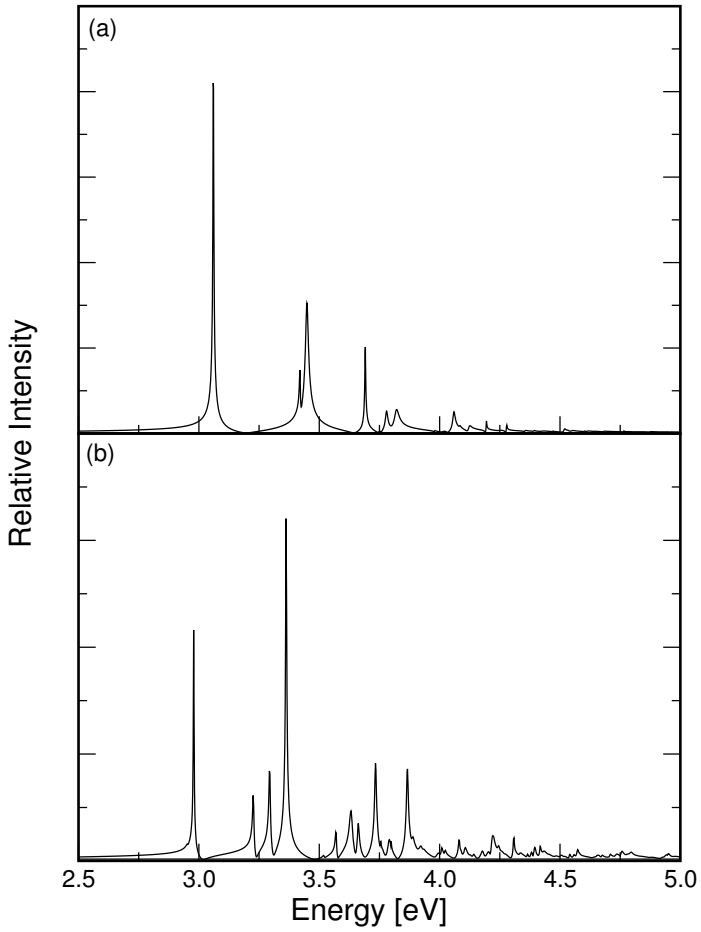

Figure A.9:

The pseudospectra of the upper adiabatic sheet, V_+, of the 3p (E') electronic manifold in the uncoupled and coupled state situations obtained with the initial GWP No. 3 (cf. Table I) are shown in Figs. 9(a-b), respectively. The band origin in the coupled state results shifts by ~ 0.08 eV to the lower energy. The width of the peaks in the two spectra essentially remains the same. The line density in the coupled state spectrum is heigher than the uncoupled one. As mentioned above the additional peaks originate from the nonadiabatic interactions in the coupled state situation. The energy eigenvalues of some of the low-lying vibronic levels of V_+ are given in Table III. The eigenfunctions of the vibrational levels of the uncoupled V_+ surface are shown in Figs. 10 (a-g). The probability density ($|\psi_n(E)|^2$) averaged over either γ or r are plotted as contour line diagrams in the (R, r) (panels in the left column) and (γ, r) plane (panels in the right column), respectively. The eigenfunctions are assigned in terms of (n_R, n_r, n_γ) specifications (as discussed above) and are included in Table III. In this case also the eigenfunctions show even quanta excitation along the angle γ. The eigenfunction in Fig. 10(c) exhibits one quantum excitation along the breathing mode and two quanta excitation along γ. The eigenfunction in Fig. 10(e) on the other hand reveals one quantum excitation along the bending mode and two quanta excitation along γ. Therefore, roughly each quantum along this degenerate vibrational mode amounts to ~ 0.57 eV.

To this end we devote some space to further discuss the coupled state results shown in Figs. 7(b) and 9(b). These two spectra are obtained with the same GWP No. 3 (cf. Table I) evolving on the same final electronic manifold. However, the differences seen in the two spectra arise due to a difference in the initial location of the GWP. In the former case it is located on V_- and in the latter case it is on V_+. Therefore, the initial location of the WP represents different admixture of the two

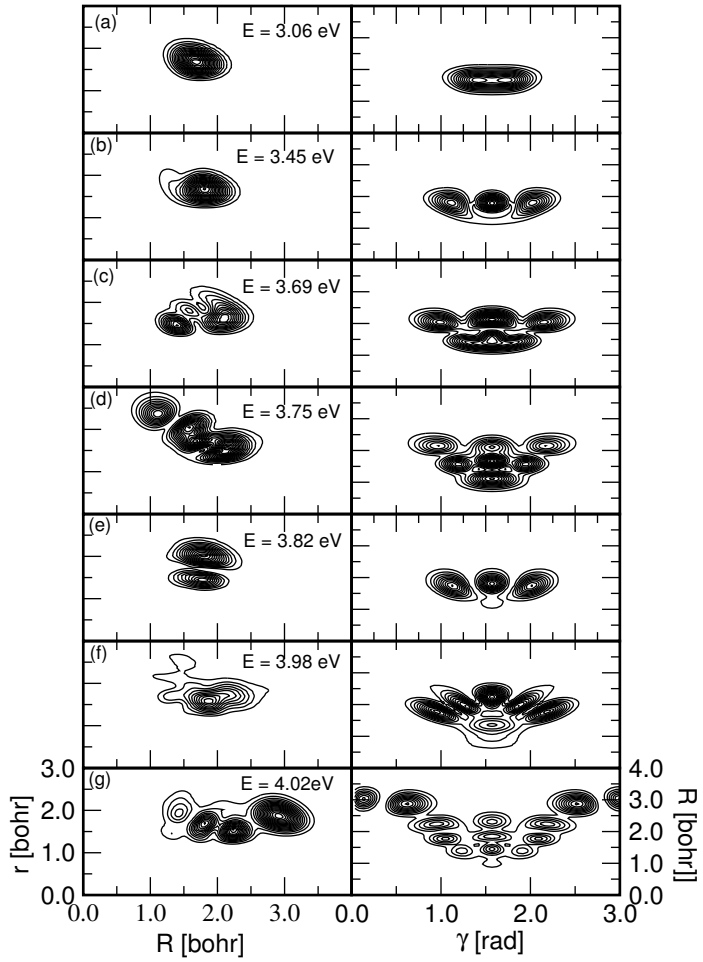
(a)
E = 3.06 eV
(b)
E = 3.45 eV
(c)
E = 3.69 eV
(d)
E = 3.75 eV
(e)
E = 3.82 eV
(f)
E = 3.98 eV
(g)
E = 4.02eV
r [bohr]
R [bohr]
γ [rad]
R [bohr]
0.0
1.0
2.0
3.0
4.0

Figure A.10:

component diabatic electronic states U_{11} and U_{22}. The energy eigenvalues of the peak maximum of the coupled state spectra are also given in Table III. It can be seen that the peaks in both the coupled state spectra appear at the same energy. However, due to two different locations of the initial WP the intensity of the peaks differs in two spectra. For example, the line at 2.95 eV gets more intensity and the line at 2.98 eV appears as a kink in Fig. 7(b), whereas the opposite trend can be observed in Fig. 9(b). As expected, the 0-0 line lies almost half-way between the 0-0 lines of the two uncoupled state spectra (cf. Table III). It is noteworthy that the coupled state energy levels do not correspond to the uncoupled ones in the same line in Table III. The additional peaks in the coupled state spectrum result from the nonadiabatic interactions between the JT split potential energy surfaces. The shift in energy of the peaks between the uncoupled and coupled state spectra is quite small. This reflects that the JT coupling in this Rydberg electronic state is rather weak compared to the far stronger coupling effects observed in the 2p (E') ground electronic state of H_3 [95, 168, 168].

A.4.2 Vibronic levels of the 3d (E'') Rydberg electronic manifold

It can be seen from Figs. 4 and 5 that the two components of the 3d (E'') electronic manifold have almost identical topography. The adiabatic and the diabatic surfaces nearly coincide in this case. The vibronic structures of both the adiabatic surfaces are found to be very similar and we show only one of them below. In Figs. 11(a-b) the vibronic structure of the upper adiabatic (V_+) state of the 3d (E'') electronic manifold in the uncoupled (panel a) and coupled (panel b) state situations is shown. These pseudospectra are calculated using the initial GWP No. 2 (cf. Table II). A close look at the spectra in panels a and b reveals

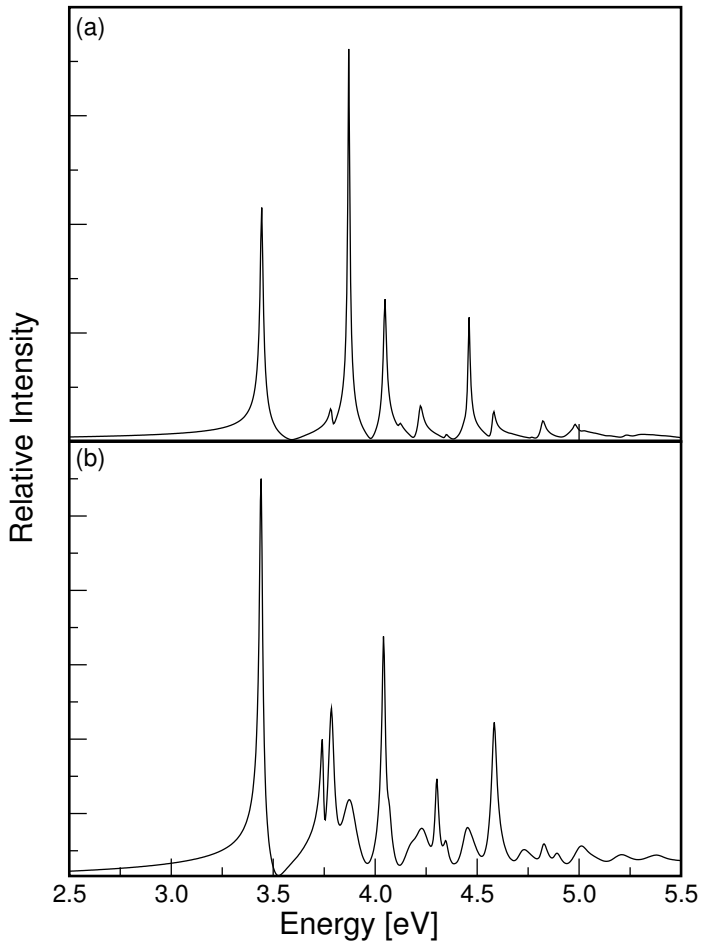

Figure A.11:

that nonadiabatic interactions cause somewhat broadening of the coupled state spectrum (panel b) at high energies. Analogous to the 3p (E') spectra, in this case also, the zero point vibrational level appears above the minimum of the seam of conical intersections at ~ 2.87 eV. The individual peak positions remain identical in both cases (cf. Table III), however, additional peaks appear due to the nonadiabatic interactions in the coupled state situation [10]. The energy eigenvalues of both the adiabatic sheets of the 3d (E'') electronic manifold in the uncoupled and coupled state situations are given in Table III.

The eigenfunctions of the low-lying vibrational levels of the uncoupled upper adiabatic sheet of the 3d (E'') electronic manifold are shown Figs. 12(a-g). They are also assigned in terms of the (n_R, n_r, n_γ) specifications discussed above and the assignments are given in Table III. The vibrational levels of the uncoupled lower adiabatic sheet reveal identical nodal progressions and we do not show them here. The eigenfunction in Fig. 12(b) seems to reveal one quantum excitation along the degenerate bending vibrational mode. The quantum of this bending vibration therefore amounts to ~ 0.43 eV, which can be compared with a value ~ 0.31 eV derived from the available experimental results [171–173]. The eigenfunction in Fig. 12(d) corresponds to one quantum excitation along both the breathing and bending vibrational modes. From the data given in Table III one can see that one quantum of the breathing vibrational mode amounts to ~ 0.35 eV. This can be compared with a value of ~ 0.39 eV estimated from the available experimental data [171–173].

More recent and improved electronic structure calculations [182] indicate a lowering of the absolute energies of the Rydberg electronic states. At the equilibrium geometry of H_3^+, the energy of the 3p (E') state is found to be ~ 0.17 eV and that of 3d (E'') state found to be ~ 0.12 eV lower than the results discussed above. In view of these corrections the energy of the minimum of the seam of intersections occurs at ~ 2.26 eV and ~ 2.76 eV for the 3p (E') and 3d (E'') electronic states, respectively. The energies of the first few vibronic levels of 3p (E') and the 3d (E'') electronic states along with the available experimental results [171–174] are given in table IV. The theoretical results in the latter are obtained by incorporating the above energy correction to the energies of table III. It can be seen that the low-lying vibronic levels of both the electronic states are in fairly good agreement with the experimental results. A more rigorous comparison

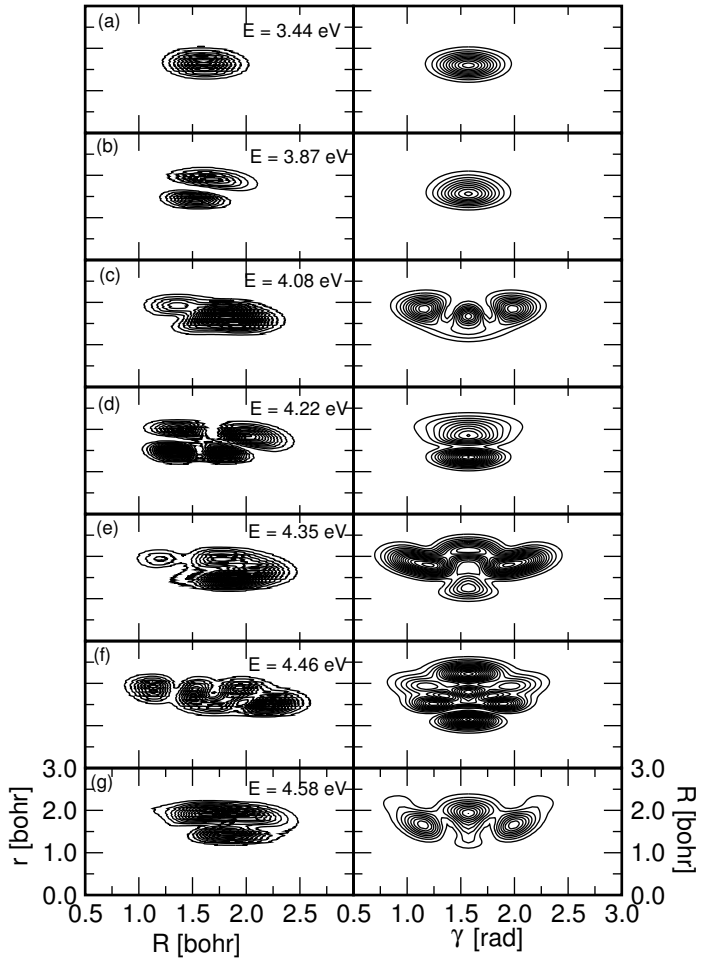
(a)
E = 3.44 eV
(b)
E = 3.87 eV
(c)
E = 4.08 eV
(d)
E = 4.22 eV
(e)
E = 4.35 eV
(f)
E = 4.46 eV
(g)
E = 4.58 eV
r [bohr]
R [bohr]
γ [rad]
R [bohr]
0.0
1.0
2.0
3.0
0.5
1.0
1.5
2.0
2.5
3.0

Figure A.12:

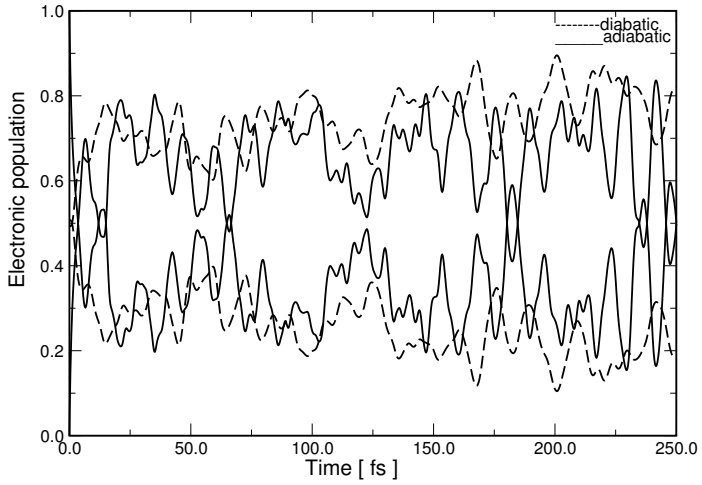

Figure A.13:

with the available experimental data [171–174] necessitates the energy levels to be calculated including the rotation, i.e., for the total angular momentum $\mathbf{J} \neq 0$. Such calculations are presently being taken up.

A.4.3 Time-dependent wave packet dynamics

We now focus on the internal conversion dynamics of the 3p (E') and 3d (E'') Rydberg electronic manifold of H_3 driven by the JT conical intersections in the respective states. The relevant quantity reported here is the time-dependence of the diabatic and adiabatic electronic populations of these states.

In Fig. 13, we show the time-dependence of the adiabatic and diabatic electronic populations in the coupled state dynamics of the 3p (E') electronic manifold. These populations and all later ones shown below represent the fractional populations. The initial GWP No. 3 (cf. Table I) is located on the upper adiabatic sheet V_+. The nuclear dynamics in this sheet is expected to be strongly affected by the nonadiabatic interactions. This is because the minimum of the

seam of conical intersections coincides with the energetic minimum of this state. The adiabatic and diabatic electronic populations in Fig. 13 are indicated by the solid and dashed lines, respectively. The upper solid curve indicates the population of V_+ and the lower one that of V_-. Since the WP is initially located on V_+, the population of this state is 1.0 at t = 0. The population of this state sharply decreases to ~ 0.5 within 3.58 fs and to ~ 0.3 within ~ 6.5 fs and then fluctuates statistically around a value of ~ 0.3 at longer times. Therefore, within ~ 3.58 fs the WP reaches the conical intersection, which is also marked by the growth of the population of V_- (upper solid line) within this period. The latter fluctuates around a value of $\sim$ of 0.7 at longer times. This indicates that on the average only 70 % of the WP reaches the lower adiabatic sheet. The maximum population exchange occurs at ~ 30 fs. Within this time ~ 80 % of the WP moves to V_-. The initial location of the WP on V_+ corresponds to an admixture of both the component diabatic states. Therefore, one finds a 49 % (51 %) population on U_{11} (U_{22}) at t = 0. The lower adiabatic surface exhibits a "Mexican hat" type of topography and has a cusp like behavior at the intersection seam. The resulting anharmonicity of this surface apparently causes most of the damping of the oscillations in the diabatic population [174] . Similar electronic population dynamics is observed by preparing the initial GWP on the lower adiabatic sheet (V_-). In this case on the average 30 % of the lower adiabatic population moves to the upper adiabatic sheet.

In order to better understand the above population dynamics we present snapshots of the WP evolving on the coupled 3p (E') electronic manifold at different times in Fig. 14. The probability density of the WP averaged over the angular coordinate is superimposed on the potential energy contours for $\gamma = \pi/2$ in the (R, r) plane. The seam of conical intersections between these two electronic states

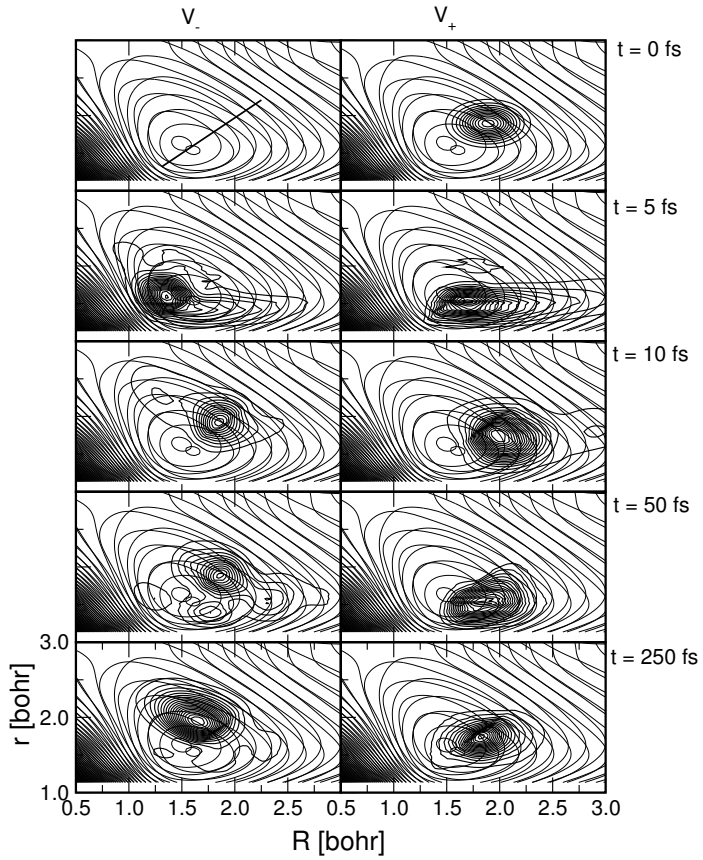
V-
V+
t = 0 fs
t = 5 fs
t = 10 fs
t = 50 fs
t = 250 fs
r [bohr]
3.0
2.0
1.0
0.5 1.0 1.5 2.0 2.5 0.5 1.0 1.5 2.0 2.5 3.0
R [bohr]

Figure A.14:

is also indicated in the first panel of the left column. It can be seen that the WP at t = 0 is generated very near to this seam. Because of this a considerable portion ($\sim$ 65 %) of the WP moves to the lower adiabatic state within $\sim$ 5 fs. (Since the WP is initially located on V_+, the population of this state is 1.0 and that of V_- is 0.0 at t = 0). Within $\sim$ 5 fs significant portion of the WP approaches the conical intersections and moves towards the minimum of the lower adiabatic sheet. The WP on V_- then moves towards the intersection seam and a portion of it moves back to V_+, which is marked by a rise in the population of the latter to $\sim$ 47 % (cf. Fig. 13) at $\sim$ 50 fs. The WP moves back and forth between the two states in time and the population exchange through the intersection seam continues. At longer times e.g., $\sim$ 250 fs, $\sim$ 76 % of the WP moves to V_-.

The electronic population dynamics in the coupled 3d (E'') electronic manifold exhibits very similar pattern as that in the 3p (E') electronic manifold. In this case the time-dependence of the populations reveal a more regular pattern. The time-dependence of the adiabatic and diabatic electronic populations obtained by locating the initial GWP No. 2 (cf. Table II) on the upper adiabatic sheet (V_+) of the 3d (E'') coupled electronic manifold is shown in Fig. 15.

As before the solid and dashed lines represent the adiabatic and the diabatic electronic populations, respectively. The time-dependence of the adiabatic electronic population exhibit a very regular pattern and the recurrences therein are on the average $\sim$ 9 fs spaced in time. In this case on the average $\sim$ 50 % of the WP moves to the lower adiabatic sheet. The initial location of the WP in this case corresponds to 50 % (50 %) admixture of the two diabatic electronic states. Unlike in the 3p (E') electronic manifold (cf. Fig. 13) the diabatic electronic populations in this case reveal a very simple pattern. The oscillations seen in the adiabatic electronic populations are heavily suppressed in the corresponding

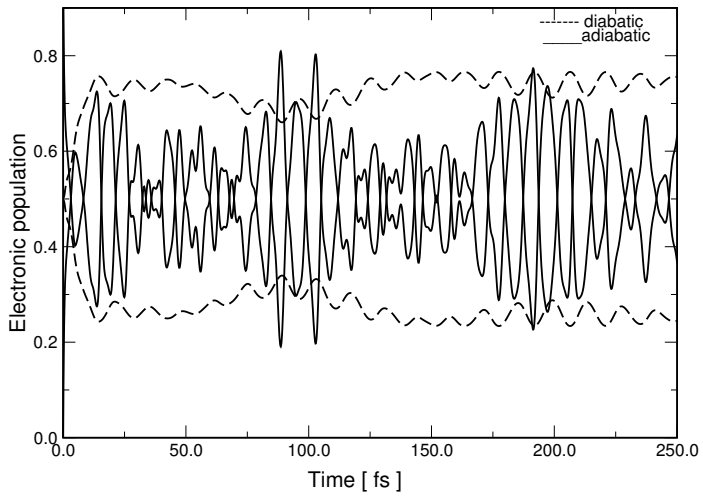

Figure A.15:

diabatic ones.

The WP motion in the above coupled 3d (E'') electronic manifold is shown in Fig. 16, at various times indicated in the diagram. The probability density of the two component adiabatic wave packets averaged over γ is plotted in the (R, r) plane and superimposed on the potential energy contours for $\gamma = \pi/2$. The seam of conical intersections is indicated by the solid line in the first panel in the left column. It can be seen that the WP is prepared close to this seam in this case also. Therefore, the WP is immediately perturbed by the strong nonadiabatic coupling and as a result $\sim$ 59 % of the WP moves to V_- at a very short time of $\sim$ 5 fs. Both the WP components move to the minimum of the respective surfaces and develop structures. The WPs move back and forth between the two states, which gives rise to quasiperiodic recurrences in the adiabatic electronic populations (cf. Fig. 15). On an average $\sim$ 50 % of the WP reaches the lower adiabatic state during the course of the entire dynamics.

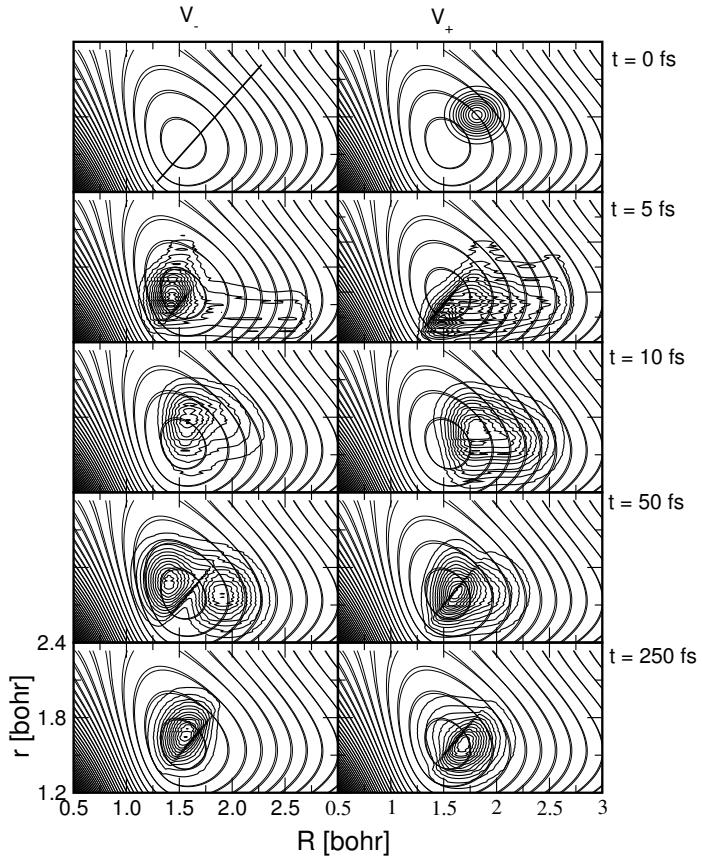
V-
V+
t = 0 fs
t = 5 fs
t = 10 fs
t = 50 fs
t = 250 fs
r [bohr]
2.4
1.8
1.2
0.5
1.0
1.5
2.0
2.5
0.5
1
1.5
2
2.5
3
R [bohr]

Figure A.16:

A.5 Summary and outlook

We have presented a detailed investigation of the topography, spectroscopy and the time-dependent dynamics of the two important degenerate 3p (E') and 3d (E'') Rydberg electronic manifolds of H_3. The static aspects of these electronic states are discussed based on the ab initio adiabatic potential energy data. The adiabatic surfaces are diabatized and the JT conical intersections are established. The spectroscopy and the time-dependent dynamics are examined by propagating the WPs on the coupled manifolds of these electronic states.

Our findings reveal that the nonadiabatic coupling effects in these Rydberg electronic manifold of H_3 are much milder than those found in case of its 2p (E') ground electronic manifold. Comparing the two Rydberg electronic states, the nonadiabatic effects are slightly stronger in case of the 3p (E') electronic manifold. It has been explained above [Eq. (11)] that the strength of the coupling potential within each electronic manifold is proportional to the splitting of the adiabatic surfaces δ and a geometrical factor. In the case of a Rydberg series this splitting is proportional to n_{eff}^{-3}, where n_{eff} is the effective principal quantum number. With n_{eff} [2p (E')] = 1.512 and n_{eff} [3p (E')] = 2.593 [180], the coupling strength is expected to be about 5 times weaker for 3p (E'), assuming a constant JT splitting if expressed by effective quantum numbers. This however is only approximately true and the real ratio of the coupling strength is $\sim 1/8$. A similar explanation can be given for even weaker coupling strength for 3d (E'') electronic manifold.

The vibronic energy levels in both uncoupled and coupled state situations have been presented here and individual eigenstates of the uncoupled adiabatic electronic states were assigned. The results compare well with the available experimental data (cf. Table IV). The present work is motivated by recent experimental interest on the dissociative recombination process of H_3. Apparently the mecha-

nism involved is much more complex and can not be satisfactorily explained by the currently available electronic structure data. An investigation of this complex mechanism and the analysis of the vibronic levels of the 3p (E') and 3d (E'') Rydberg electronic manifolds of H_3 including rotations are the two main tasks in the future and are presently in progress.

Finally we note that, a referee raised the question whether this result would contradict the important role of the JT coupling in the dissociative recombination process claimed by Greene and coworkers [51]. These authors presented a model based on multichannel quantum defect theory which treats the capture of an electron into a whole Rydberg series, distinguishing direct (2p (E')) and indirect (higher Rydberg states) processes. The present study does not deal with the process of electron capture, but the predicted probability of population for the upper and lower sheet of 3p (E') (30 % : 70 %) may be relevant, under suitable circumstances, to the branching ratio of the H + H_2 and H + H + H channels.

Table A.1: Parameters for different choices of the initial Gaussian wave packet used for simulating nuclear dynamics in the 3p (E') Rydberg electronic manifold of H_3.

GWP	R_0 (a_0)	r_0 (a_0)	γ_0 (rad)	σ_R (a_0)	σ_r (a_0)	σ_γ (rad)	$\langle E \rangle$ (eV)
1	1.5823	1.5903	1.5708	0.25	0.20	0.15	3.0895
2	1.7882	1.7899	1.5708	0.25	0.20	0.15	3.1267
3	1.8912	1.8950	1.5708	0.25	0.20	0.15	3.4231
4	1.9868	2.0105	1.5708	0.25	0.20	0.15	3.6885
5	2.0823	2.0840	1.5708	0.25	0.20	0.15	3.9243
6	2.1779	2.1786	1.5708	0.25	0.20	0.15	4.2052

Table A.2: Parameters for different choices of the initial Gaussian wave packet used for simulating nuclear dynamics in the 3d (E'') Rydberg electronic manifold of H_3.

GWP	R_0 (a_0)	r_0 (a_0)	γ_0 (rad)	σ_R (a_0)	σ_r (a_0)	σ_γ (rad)	$\langle E \rangle$ (eV)
1	1.6872	1.6876	1.5708	0.20	0.15	0.10	3.6068
2	1.8149	1.8145	1.5708	0.20	0.15	0.10	3.8071
3	1.9092	1.9095	1.5708	0.20	0.15	0.10	4.0789

Table A.3: Vibronic energy levels of the uncoupled and coupled lower (V_-) and upper (V_+) adiabatic electronic states of the 3p (E') and 3d (E'') Rydberg electronic manifolds of H_3. The assignments of the vibrational levels of the uncoupled states are also given (see text for details). A blank entry in the table implies that the corresponding quantity can not be given unambiguously.

3p (E′)						3d (E″)					
V_-			V_+			V_-			V_+		
Uncoupled		Coupled*	Uncoupled		Coupled*	Uncoupled		Coupled*	Uncoupled		Coupled*
Energy	Energy	Assignment	Energy	Energy	Assignment	Energy	Energy	Assignment	Energy		
eV	(n_R, n_r, n_γ)	eV	eV	(n_R, n_r, n_γ)	eV	eV	(n_R, n_r, n_γ)	eV	eV	(n_R, n_r, n_γ)	eV
2.91	(0,0,0)	2.95	3.06	(0,0,0)	2.95	3.44	(0,0,0)	3.44	3.44	(0,0,0)	3.44
3.29	(0,1,0)	2.98	3.45	(0,0,2)	2.98	3.87	(0,1,0)	3.74	3.87	(0,1,0)	3.74
3.43	(0,0,2)	3.22	3.69	(1,-,2)	3.22	4.04	(0,0,2)	3.78	4.04	(0,0,2)	3.78
3.48	(1,0,2)	3.29	3.75	(2,0,2)	3.29	4.22	(1,1,0)	3.87	4.22	(1,1,0)	3.87
3.56	(1,1,0)	3.36	3.82	(0,1,2)	3.36	4.35	(1,0,2)	4.03	4.35	(1,0,2)	4.03
3.66	(0,2,2)	3.57	3.98	(0,0,4)	3.57	4.46	(3,0,2)	4.22	4.46	(3,0,2)	4.22
3.79	(1,1,2)	3.64	4.02	(3,0,2)	3.64	4.58	(0,1,2)	4.31	4.58	(0,1,2)	4.31
3.90	(2,2,0)	3.67	-	-	3.67	-	-	4.33	-	-	4.45
-	-	3.74	-	-	3.74	-	-	4.45	-	-	4.55
-	-	3.80	-	-	3.80	-	-	4.55	-	-	4.59
-	-	3.86	-	-	3.86	-	-	4.59	-	-	-
-	-	3.88	-	-	3.88	-	-	-	-	-	-
-	-	3.91	-	-	3.91	-	-	-	-	-	-
-	-	3.99	-	-	3.99	-	-	-	-	-	-
-	-	4.02	-	-	4.02	-	-	-	-	-	-
-	-	4.09	-	-	4.09	-	-	-	-	-	-
-	-	4.10	-	-	4.10	-	-	-	-	-	-

*Coupled surface energy levels do not correspond to the quantum number assignments and to the uncoupled surface energy levels in the same line.

Table A.4: The low-lying vibronic levels of the 3p (E') and 3d (E'') Rydberg electronic manifolds of H_3 along with the available experimental results [176–179]. The two numbers in the parentheses in the first column indicate the quantum numbers of the breathing and bending vibrational modes, respectively. The theoretical energy values are obtained from the coupled state energies of Table III with the corrections noted in the text at the end of the section IV B. A blank entry implies the corresponding value is not available.

Vibronic level	*Theory* (eV)	*Experiment.* (eV)
3p E′(0,0)	2.79	2.72
3p E′(1,0)	3.06	–
3p E′(0,1)	3.17	3.05
3d E″(0,0)	3.32	3.26
3d E″(1,0)	3.67	3.65
3d E″(0,1)	3.66	3.56

Bibliography

[1] M. Born and E. Oppenheimer, Ann. Phys. **84**, 457 (1927).

[2] M. Born and K. Huang, in *The Dynamical Theory of Cryatal Lattices* (Oxford University Press, 1954).

[3] Chemical Physics **259**, 121-350, 2000 (special issue on conical intersections)

[4] W. Domcke, D. R. Yarkony, H. Köppel, Eds. *Conical Intersections: Electronic Structure, Dynamics and Spectroscopy*, (World Scientific, Singapore 2004).

[5] D. R. Yarkony, Rev. Mod. Phys. **68**, 985 (1996).

[6] H. Jahn and E. Teller, Proc. Roy. Soc. London, Ser. A. **161**, 220 (1937).

[7] I. B. Bersuker, *The Jahn - Teller Effect and Vibronic Interactions in Modern Chemistry* (Plenum Press, New York, 1984).

[8] R. Englman, *The Jahn - Teller Effect in Molecules and Crystals*, (Wiley, New York, 1972).

[9] I. B. Bersuker, Chem. Rev., **101**, 1067 (2001).

[10] H. Köppel, W. Domcke and L. S. Cederbaum, Adv. Chem. Phys., **57**, 59 (1984).

[11] M. Z. Zgierski and M. Pawlikowski, J. Chem. Phys., **70**, 3444 (1979).

[12] H. Köppel, L. S. Cederbaum and W. Domcke, J. Chem. Phys., **89**, 2023 (1988).

[13] H. Köppel, L. S. Cederbaum and W. Domcke, J. Chem. Phys., **111**, 10452 (1988).

[14] E. Renner, Z. Phys., **92**, 172 (1934).

[15] Ch. Jungen and A. Merer, J. Mol. Phys., **40**, 1 (1980).

[16]

[17] *Conical intersections in photochemistry, spectroscopy and chemical physics*, Chem. Phys., **259** (2000).

[18] T. F. O'Malley, Phys. Rev., **162**, 98 (1967).

[19] W. Lichten, Phys. Rev., **164**, 131 (1967).

[20] F. T. Smith, Phys. Rev., **179**, 111 (1969).

[21] T. Pacher, L. S. Cederbaum and H. Köppel, Adv. Chem. Phys., **84**, 293 (1993).

[22] A. Thiel and H. Köppel, J. Chem. Phys., **110**, 9371 (1999).

[23] H. Köppel, J. Gronki and S. Mahapatra, J. Chem. Phys., **115**, 23771 (2001).

[24] S. Mahapatra, H. Köppel and L. S. Cederbaum, J. Phys. Chem. A, **105**, 2321 (2001).

[25] F. Fernández-Alonso and R. N. Zare, Ann. Rev. Phys. Chem. **53**, 67 (2002).

[26] F. J. Aoiz, L. Bañares and V. J. Herrero, Int. Rev. Phys. Chem. **24**, 119 (2005).

[27] F. London, *Z. Elektrochem*, **35**, 552 (1929).

[28] D. G. Truhlar and R. E. Wyatt, Annu. Rev. Phys. Chem., **27**, 1 (1976).

[29] G. C. Schatz, Annu. Rev. Phys. Chem., **39**, 317 (1988).

[30] D. E. Manolopoulos and R. E. Wyatt, J. Chem. Phys. **92**, 810 (1990).

[31] J. Chang and N. J. Brown, J. Chem. Phys. **103**, 4097 (1995).

[32] D. M. Charutz, I. Last and M. Baer, J. Chem. Phys. 106, 7654 (1997).

[33] L. Bañares, F. J. Aoiz, V. J. Herrero, M. J. D'Mello, B. Niederjohann, K. Seekamp-Rahn, E. Wrede and L. Schnieder, J. Chem. Phys. **108**, 6160 (1998).

[34] S. Sukiasyan and H. D. Meyer, J. Chem. Phys. **116**, 10641 (2002).

[35] A. Jäckle and H. D. Meyer, J. Chem. Phys. **109**, 2614 (1998).

[36] B. K. Kendrick, J. Chem. Phys. **114**, 8796 (2001).

[37] B. D. Bean, J. D. Ayers, F. Fernández-Alonso, and R. N. Zare, J. Chem. Phys. **116**, 6634 (2002).

[38] S. C. Althorpe, J. Chem. Phys. **117**, 4623 (2002).

[39] S. C. Althorpe, F. Fernández-Alonso, B. D. Bean, J. D. Ayers, A. E. Pomerantz, R. N. Zare and E. Wrede, Nature (London) **416**, 67 (2002).

[40] S. A. Harich, D. Dai, C. C. Wang, X. Yang, S. D. Chao and R. T. Skodje, Nature (London) **419**, 281 (2002).

[41] S. L. Mielke, K. A. Peterson, D. Q. Schuenke, B. C. Garrett, D. G. Truhlar, J. V. Michael, M. C. Su, and J. W. Sutherland, Phys. Rev. Lett. **91**, 063201 (2003).

[42] D. X. Dai, C. C. Wang, S. A. Harich, X. Y. Wang, X. M. Yang, S. D. Chao and R. T. Skodje, Science **300**, 1730 (2003).

[43] F. Ausfelder, A. E. Pomerantz, R. N. Zare, S. C. Althorpe, F. J. Aoiz, L. Bañares, and J. F. Castillo, J. Chem. Phys. **120**, 3255 (2004).

[44] K. Koszinowski, N. T. Goldberg, J. Zhang, R. N. Zare, F. Bouakline, and S. C. Althorpe, J. Chem. Phys. (in press).

[45] K. Koszinowski, N. T. Goldberg, A. E. Pomerantz and R. N . Zare, J. Chem. Phys., **123**, 054306-1 (2005); A. E. Pomerantz, F. Ausfelder, R. N . Zare, S. C. Althorpe, F. J. Aoiz, L. Bañares and J. F. Castillo, J. Chem. Phys., **120**,3244 (2004); **120**, 3255 (2004).

[46] C. A. Mead, J. Chem. Phys., **72**, 3839 (1980).

[47] D. G. Truhlar and R. E. Wyatt, Ann. Rev. Phys. Chem. **27**, 1 (1976); G. Herzberg, *ibid.* **38**, 27 (1987); W. H. Miller, *ibid.* **41**, 245 (1990).

[48] I. F. Schneider and A. E. Orel, J. Chem. Phys. **96**, 4283 (1992).

[49] J. L. Krause, K. C. Kulander, J. C. Light and A. E. Orel, J. Chem. Phys. **96**, 4283 (1992); A. E. Orel, I. F. Schneider and A. Suzor-Weiner, Phil. Trans. R. Soc. Lon. **A 358**, 2445 (2000).

[50] B. J. McCall and T. Oka, Science, **287**, 1941, (2000).

[51] V. Kokoouline, Chris H. Greene and B. D. Esry, Nature, **412**, 891 (2001); V. Kokoouline and Chris H. Greene, Faraday Discuss. **127**, 413 (2004); Phy. Rev. Lett. **90**, 133201 (2003).

[52] Dissociative Recombination: theory, experiment and application, IV, Eds. M. Larsson, J. B. A. Mitchell and I. F. Schneider (World Scientific, Singapore, 2000).

[53] M. Larsson, Philos. Trans. R. Soc. London, Ser. A **358**, 2433 (2000); B. J. McCall et al., Nature (London) **422**, 500 (2003); V. Poterya, J. Glosik, R. Plasil, M. Tichy, P. Kudrna, and A. Pysanenko, Phys. Rev. Lett. **88**, 044802 (2002); V. Kokoouline and C. H. Greene, Phys. Rev. A **68**, 012703 (2003).

[54] B. J. McCall, T. R. Geballe, K. H. Hinkle and T. Oka, Science, **279**, 1910 (1998).

[55] D. G. Truhlar and C. J. Horowitz, J. Chem. Phys., **68**, 2466 (1978).

[56] D. G. Truhlar and C. J. Horowitz, J. Chem. Phys, **71**, 1514 (1979).

[57] A. J. C. Varandas, F. B. Brown, C. A. Mead, D. G. Truhlar and N. C. Blais, J. Chem. Phys, 86, **6258** (1987).

[58] A. L. Boothroyd, W. J. Keogh, P. G. Martin and M. R. Peterson, J. Chem. Phys, **95**, 4343 (1996).

[59] A. L. Boothroyd, W. J. Keogh, P. G. Martin and M. R. Peterson, J. Chem. Phys, **104**, 7139 (1991).

[60] B. Liu, J. Chem. Phys., **58**, 1925 (1973).

[61] P. E. M. Siegbahn and B. Liu, J. Chem. Phys., **68**, 2457 (1978).

[62] M. R. A. Blomberg and B. Liu, J. Chem. Phys., **82**, 1050 (1985).

[63] B. O. Roos, P. R. Taylor and P. E. M. Siegbahn, Chem. Phys., **48**, 157 (1980).

[64] R. N. Porter, R. M. Stevens and M. Karplus, J. Chem. Phys., **49**, 5163 (1968).

[65] T. C. Thompson and C. A. Mead, J. Chem. Phys., **82**, 2408 (1985).

[66] T. C. Thompson, G. Izmirlian Jr., S. J. Lemon, D. G. Truhlar and C. A. Mead, J. Chem. Phys., **82**, 5597 (1985).

[67] K. D. Jordon, Chem. Phys., **9**, 199 (1975).

[68] Y. -S. M. Wu, A. Kuppermann and J. B. Anderson, Phys. Chem. Chem. Phys., **1**, 929 (1999).

[69] S. L. Mielke, B. C. Garrett and K. A. Peterson, J. Chem. Phys., **116**, 4142 (2002).

[70] B. Jayachander Rao, R. Padmanaban and S. Mahapatra, Chem. Phys., **333**, 135 (2007).

[71] S. Ghosal, B. Jayachander Rao and S. Mahapatra, J. Chem. Sci., **119**, 401 (2007).

[72] B. Jayachander Rao and S. Mahapatra, Indian. J. Phys., **81**, 1003 (2007).

[73] J. C. Juanes-Marcos and S. C. Althorpe, Chem. Phys. Lett., **381**, 743 (2003).

[74] J. C. Juanes-Marcos and S. C. Althorpe, J. Chem. Phys., **122**, 204324 (2005).

[75] J. C. Juanes-Marcos, S. C. Althorpe and E. Wrede, Science, **309**, 1227 (2004).

[76] S. C. Althorpe, J. Chem. Phys., **124**, 084105 (2006); ibid, **126**, 044317 (2007).

[77] G. Herzberg, H. C. Longuet-Higgins, Disscuss. Faraday. Soc., **35**, 77 (1963).

[78] B. Lepetit, A. Kuppermann, Chem. Phys. Lett., **166**, 581 (1979).

[79] Y. M. Wu, A. Kuppermann and B. Lepetit, Chem. Phys. Lett, 186, 319 (1991).

[80] A. Kuppermann and Y. M. Wu, Chem. Phys. Lett, **205**, 577 (1993).

[81] A. Kuppermann and Y. M. Wu, Chem. Phys. Lett, **241**, 229 (1995).

[82] A. Kuppermann and Y. M. Wu, Chem. Phys. Lett, **349**, 537 (2001).

[83] C. A. Mead and D. G. Truhlar, J. Chem. Phys., **70**, 2284 (1979).

[84] C. A. Mead, J. Chem. Phys., **72**, 3839 (1980).

[85] D. A. Kliner, D. E. Adelman and R. N. Zare, J. Chem. Phys., **95**, 1648 (1991).

[86] E. Wrede, L. Schnieder, K. H. Welge, F. J. Aoiz, L. Bañares, V. J. Herrero, B. Martínez-Haya and V. Sáez Rábanos, J. Chem. Phys., **106**, 7862 (1997).

[87] B. K. Kendrick, J. Chem. Phys., **112**, 5679 (2000).

[88] B. K. Kendrick, J. Chem. Phys., **114**, 4335 (2001).

[89] B. K. Kendrick, J. Phys. Chem. A, **107**, 6739 (2003).

[90] B. K. Kendrick, J. Chem. Phys., **118**, 10502 (2003).

[91] B. K. Kendrick, J. Chem. Phys., **114**, 8796 (2001).

[92] A. J. C. Varandas and H. G. Yu, Faraday Trans. **93** 819 (1997).

[93] R. Bruckmeier, Ch. Wunderlinch, H. Figger, Phys. Rev. Lett., **72**, 2250 (1994).

[94] D. Azinovic, R. Bruckmeier, Ch. Wunderlich, H. Figger, G. Theodorakopoulos and I. D. Petsalakis, Phys. Rev. A., **58**, 1115 (1998).

[95] S. Mahapatra and H. Köppel, Phys. Rev. Lett., **81**, 3116 (1998).

[96] E. J. Rackham, F. Huarte-Larranaga and D. E. Manolopoulos, Chem. Phys. Lett. **343**, 356 (2001).

[97] E. J. Rackham, T. Gonzalez-Lezana and D. E. Manolopoulos, J. Chem. Phys. **119**, 12895 (2003).

[98] D. C. Clary and J. P. Henshaw, Faraday Discuss. Chem. Soc. **84**, 333 (1987).

[99] P. Honvault and J.-M. Launay, J. Chem. Phys. **111**, 6665 (1999).

[100] P. Honvault and J.-M. Launay, J. Chem. Phys. **114**, 1057 (2001).

[101] N. Balucani, L. Cartechini, G. Capozza, E. Segoloni, P. Casavecchia, G. G. Volpi, F. J. Aoiz, L. Bañares, P. Honvault and J.-M. Launay, Phys. Rev. Lett. **89**, 013201 (2002).

[102] A. N. Wright and C. A. Winkler, *Active Nitrogen*; Academic Press: New York, 1968; W. R. Anderson and A. Fontijn, Gas-phase kinetics for propellant combustion modelling: Requirements and experiments, in: R. W. Shaw, T. B. Brill and D. L. Thompson (Eds.), *Overviews of recent research on energetic materials*, World Scientific, Singapore, 2005, p. 192.

[103] T. Suzuki, Y. Shihira, T. Sato and S. Tsunashima, J. Chem. Soc. Faraday Trans., **89**, 995 (1993).

[104] H. Kobayashi, T. Takayanagi, K. Yokoyama, T. Sato and S. Tsunashima, J. Chem. Soc. Faraday Trans., **91**, 3771 (1995).

[105] J. A. Dodd, S. J. Lipson, D. J. Flanagan, W. A. M. Blumberg, J. C. Pearson and B. D. Green, J. Chem. Phys., **94**, 4301 (1991).

[106] H. Umemoto and K. Matsumoto, J. Chem. Phys., **104**, 9640 (1996).

[107] H. Umemoto, T. Asai and Y. Kimura, J. Chem. Phys. **106**, 4985 (1997).

[108] M. Alagia, N. Balucani, L. Cartechini, P. Cachavecchia, G. G. Volpi, L. A. Pederson, G. C. Scatz, G. Lendavy, L. B. Harding, T. Hollenbeek, T. -S. Ho and H. Rabitz, J. Chem. Phys. **119**, 3063 (2003).

[109] T. -S. Ho, H. Rabitz, F. J. Aoiz, L. Bañares, S. A. Vázquez and L. B. Harding, J. Chem. Phys., **119**, 3063 (2003).

[110] S. Y. Lin and H. Guo, J. Chem. Phys., **124**, 031101 (2006).

[111] S. Y. Lin and H. Guo, Phys. Rev. A **74**, 022703 (2006).

[112] S. Y. Lin, L. Bañares and H. Guo, J. Phys. Chem. A, (2007), 10.1021/jp0682715.

[113] A. J. C. Varandas and L. A. Poveda, Theor. Chem. Acc., **116**, 404 (2006).

[114] T. S. Chu, K. L. Han and A. J. C. Varandas, J. Phys. Chem. A., **110**, 1666 (2006).

[115] J. F. Castillo, N. Bulut, L. Bañares and F. Gogtas, Chem. Phys., **332**, 119 (2007).

[116] S. K. Gray, G. G. Balint-Kurti, J. Chem. Phys. **108**, 950 (1998).

[117] J. M. Bowman, J. Phys. Chem. **95**, 4960 (1991).

[118] (a)S. L. Mielke, G. C. Lynch and D. G. Truhlar, J. Phys. Chem., **98**, 8000 (1994); (b)D. H. Zhang, J. Z. H. Zhang, J. Chem. Phys. **110**, 7622 (1999).

[119] N. Aronszajn, Trans. Am. Math. Soc., **68**, 337 (1950).

[120] C. de Boor and R. Lynch, J. Math. Mech., **15**, 953 (1966).

[121] P. J. Davis, *Interpolation and approximation*, Dover, New York (1975).

[122] L. A. Pederson, G. C. Schatz, T. Ho, T. Hollenbeek, H. Rabitz and L. B. Harding, J. Chem. Phys., **110**, 9091 (1999).

[123] K. Dressler and D. A. Ramsay, Philos. Trans. R. Soc. London, Ser. A **51**, 553 (1959).

[124] F. Santoro, C. Petrongolo and G. C. Schatz, J. Phys. Chem., A **106**, 8276 (2002).

[125] P. Defazio and C. Petrongolo, J. Chem. Phys., **125**, 064308 (2006).

[126] L. Adam, W. Hack, G. C. MacBane, H. Zhu, Z.-W. Qu and R. Schinke, J. Chem. Phys. **126**, 034304 (2007).

[127] R. F. Lu, T. S. Chu, Y. Zhang, K. L. Han, A. J. C. Varandas and J. Z. H. Zhang, J. Chem. Phys., **125**, 133108 (2006).

[128] T. S. Chu, K. L. Han, M. Hankel and G. G. Balint-Kurti, J. Chem. Phys., **126**, 214303 (2007).

[129] M. Hankel, S. C. Smith, R. J. Allan, S. K. Gray and G. G. Balint-Kurti, J. Chem. Phys., **125**, 164303 (2006).

[130] P. Defazio and C. Petrongolo, J. Chem. Phys., **127**, 204311-1 (2007).

[131] D. Kosloff and R. Kosloff, Comput. Phys. Commun., **30**, 333 (1983); J. Chem. Phys., **52**, 35 (1983).

[132] R. Kosloff, J. Phys. Chem., **92**, 2087 (1988); Ann. Rev. Phys. Chem., **45**, 145 (1994), and references therein.

[133] R. T. Pack, J. Chem. Phys., **60**, 633 (1974).

[134] P. McGuire and D. J. Kouri, J. Chem. Phys., **60**, 2488 (1974).

[135] D. T. Colbert and W. H. Miller, J. Chem. Phys. **96**, 1982 (1992).

[136] A. Askar and A. S. Cakmak, J. Chem. Phys. **68**, 2794 (1978); D. Kosloff and R. Kosloff, Comput. Phys. Commun. **30**, 333 (1983); J. Chem. Phys. **52**, 35 (1983).

[137] M. D. Feit, J. A. Fleck Jr. and A. Steiger, J. Comput. Phys. 47, 412 (1982).

[138] H. Tal-Ezer and R. Kosloff, J. Chem. Phys., **81**, 3967 (1984).

[139] T. J. Park and J. C. Light, J. Chem. Phys. **85**, 5870 (1986).

[140] G. Arfken, *Mathematical Methods for Physicists*, Academic Press Inc., Prism Books Pvt. Ltd., Bangalore, (1994).

[141] R. Kosloff, J. Phys. Chem., **92**, 2087 (1988).

[142] V. Mohan and N. Sathyamurthy, Comput. Phys. Rep., **7**, 213 (1988).

[143] R. Kosloff, Ann. Rev. Phys. Chem., **45**, 145 (1994).

[144] D. Kosloff and R. Kosloff, J. Comput. Phys., **52**, 35 (1983).

[145] J. C. Light, I. P. Hamilton, J. V. Lill, J. Chem. Phys. **82**,1400 (1985). Z. Bačić, J. C. Light, Ann. Rev. Phys. Chem. **40**, 469 (1989).

[146] G. C. Corey and D. Lemoine, J. Chem. Phys. **97**, 4115 (1992).

[147] A. R. Offer and G. G. Balint-Kurti, J. Chem. Phys. **101**, 10416 (1994).

[148] D. Neuhauser and M. Baer, J. Phys. Chem. **93**, 2872 (1989); J. Chem. Phys. **91**, 4651 (1989); D. Neuhauser, M. Baer, R. S. Judson and D. J. Kouri, Comput. Phys. Commun. **63**, 460 (1991).

[149] S. Mahapatra and N. Sathyamurthy, J. Chem. Soc., Faraday Trans. **93**, 773 (1997).

[150] J. Z. H. Zhang, Theory and Application of Quantum Molecular Dynamics; World Scientifc, Singapore, 1999.

[151] F. J. Aoiz, L. Bañares, and J. F. Castillo, J. Chem. Phys. **111**, 4013 (1999).

[152] W. H. Press, B. P. Flannery,S. A. Teukolsky, W. T. Vetterling, Numerical Recipes in Fortran: The Art of Scientifc Computing, 2nd ed.; Cambridge University Press: New York.

[153] F. J. Aoiz, M. Brouard, C. J. Eyles, J. F. Castillo and V. S. Rãbanos, J. Chem. Phys. **125**, 144105 (2006).

[154] S. Sukiasyan and H. -D. Meyer, J. Chem. Phys., **116**, 10641 (2002).

[155] T. J. Park and J. C. Light, J. Chem. Phys. **91**, 974 (1992).

[156] *Dynamics of Molecules and Chemical Reactions*, edited by R. E. Wyatt and J. Z. H. Zhang (Marcel Dekker, New York, 1996).

[157] (a) N. Balakrishnan, C. Kalyanaraman, N. Sathyamurthy, Phys. Rep. **280**, 79, (1997); (b) M. Beck, A. Jäckle, G. A. Worth, and H. -D. Mayer, Phys. Rep. **324**, 1, (2000); (c) G. Nyman and H. -G. Yu, Rep. Prog. Phys. **63**, 1001 (2000).

[158] R. Skodje, R. Sadeghi, H. Kppel and J. Krause, J. Chem. Phys., **101**, 1725 (1994).

[159] S. K. Gray, E. M. Goldfield, G. C. Schatz and G. G. Balint-Kurti, Phys. Chem. Chem. Phys., **1**, 1141 (1999).

[160] F. Fernández-Alonso and R. N. Zare, Annu. Rev. Phys. Chem., **53**, 67 (2002).

[161] U. Manthe, H.-D. Mayer, and L. S. Cederbaum, J. Chem. Phys. **97**, 9062 (1992); V. Engel, Chem. Phys. Lett. **189**, 76 (1992).

[162] R. Sadeghi and R. T. Skodje, J. Chem. Phys. **102**, 193 (1995).

[163] S. Mahapatra and N. Sathyamurthy, J. Chem. Phys. **105**, 10934 (1996).

[164] M. L. Mehta, *Random Matrices*, 2^{nd} ed. (Academic. New York).

[165] M. V. Berry and M. Tabor, Proc. R. Soc. London, Ser. **A 356**, 375 (1977).

[166] T. A. Brody, J. Flores, J. B. French, P. A. Mello, A. Pandey, and S. S. M.Wong, Rev. Mod. Phys. **53**, 385 (1981).

[167] M. V. Berry and M. Robnik, J. Phys. **A 17**, 2413 (1984).

[168] S. Mahapatra and H. Köppel, J. Chem. Phys. **109**, 1721 (1998).

[169] M. Jungen, M. Lehner and R. Guérout, Khimicheskaya Fizika **23(2)**, 71 (2004);(an electronic copy of the same can be obtained from the author on request).

[170] S. Mahapatra and H. Köppel, Chem. Phys. Lett. **306**, 387 (1999).

[171] G. Herzberg, J. T. Hougen and J. K. G. Watson, Can. J. Phys. **60**, 1261 (1982).

[172] U. Müller and P. C. Cosby, J. Chem. Phys. **105**, 3531 (1996).

[173] W. Ketterle, H. P. Messmer and H. Walther, Europhys. Lett. **8**, 333 (1989).

[174] U. Manthe and H. Köppel, J. Chem. Phys., **93**, 345, 1685 (1990).

[175] B. Lepetit, Z. Peng and A. Kuppermann, Chem. Phys. Lett. **166**, 572 (1990)

[176] G. Herzberg, J. T. Hougen and J. K. G. Watson, Can. J. Phys. **60**, 1261 (1982).

[177] U. Müller and P. C. Cosby, J. Chem. Phys. **105**, 3531 (1996).

[178] W. Ketterle, H. P. Messmer and H. Walther, Europhys. Lett. **8**, 333 (1989).

[179] U. Galster, Private communication.

[180] I. Mistrik, R. Reichle, U. Müller, H. Helm, M. Jungen and J.A. Stephens, Phy. Rev. A **61**, 033410 (1999).

[181] J. Tennyson and B. T. Sutcliffe, J. Chem. Phys., **77**, 4061 (1982).

[182] M. Jungen, (Unpublished results).